Histol Histopathol (2025) 40: 843-856

Histology and Histopathology
From Cell Biology to Tissue Engineering

ORIGINAL ARTICLE Open Access

Time course analysis of changes in neuronal loss, oxidative stress, and excitotoxicity in gerbil hippocampus following ischemia and reperfusion under hyperthermic conditions

Tae-Kyeong Lee[1]*, Dae Won Kim[2]*, Joon Ha Park[3], Choong-Hyun Lee[4], Se-Ran Yang[5], Myoung Cheol Shin[6], Moo-Ho Won[6], Jun Hwi Cho[6] and Ji Hyeon Ahn[7]

[1]Department of Anatomy and Developmental Biology, College of Dentistry, Kyung Hee University, Seoul, [2]Department of Biochemistry and Molecular Biology, Research Institute of Oral Sciences, College of Dentistry, Gangneung-Wonju National University, Gangneung, [3]Department of Anatomy, College of Korean Medicine, Dongguk University, Gyeongju, [4]Department of Pharmacy, College of Pharmacy, Dankook University, Cheonan, [5]Department of Cardiovascular Surgery, School of Medicine, Kangwon National University, [6]Department of Emergency Medicine, Kangwon National University Hospital, School of Medicine, Kangwon National University, Chuncheon and [7]Department of Physical Therapy, College of Health Science, Youngsan University, Yangsan, Republic of Korea

*contributed equally to this work

Summary. Oxidative stress and excitotoxicity are the major causes of neuronal death/loss in the brain following ischemia and reperfusion (IR). Hyperthermia is known to exacerbate ischemic neuronal damage; however, the underlying mechanisms remain unclear. This study investigated the mechanisms underlying neuronal damage caused by IR injury (IRI) under hyperthermic conditions in the gerbil hippocampal CA1 region. Gerbils were controlled at normothermia (37.5±0.2°C) or hyperthermia (39.5±0.2°C). After temperature control for 30 min, the animals received IRI (following 5 min of transient forebrain ischemia) or sham ischemia, and were subsequently sacrificed at 0, 3, 6, 12, 24, 48, and 120h after IRI. Neuronal death was examined using neuronal nuclear antigen immunohistochemistry and Fluoro-Jade B histofluorescence. Oxidative stress was analyzed by immunohistochemistry for 8-Hydroxy-2'-deoxyguanosine (8OHdG) and superoxide dismutase 2 (SOD2). Excitotoxicity was investigated by immunohistochemistry and western blotting for glutamate transporter 1 (GLT1). Immunohistochemical staining for glial fibrillary acidic proteins (GFAP) was performed to detect reactive astrogliosis. Loss of pyramidal neurons was detected earlier (48h post-IRI) in the hyperthermia-IRI group than in the normothermia-IRI group (120h post-IRI). Further, 8OHdG and SOD2 immunoreactivity in the hyperthermia-IRI group was significantly higher than that in the normothermia-IRI group. Changes in GLT1 immunoreactivity in both groups were biphasic, indicating that the immunoreactivity and protein levels were significantly lower in the hyperthermia-IRI group. GFAP immunoreactivity was enhanced following neuronal loss, indicating that the immunoreactivity was significantly higher in the hyperthermia-IRI group. Taken together, these results suggest that brain IR under hyperthermic conditions can aggravate neuronal damage in the hippocampal CA1 region through severe oxidative stress and excitotoxicity.

Key words: Antioxidant enzyme, DNA damage, Glutamate transporters, Astrocyte, SOD2, Transient forebrain ischemia

Corresponding Author: Professor Jun Hwi Cho, MD, PhD, Department of Emergency Medicine, and Institute of Medical Sciences, Kangwon National University Hospital, School of Medicine, Kangwon National University, Chuncheon, Gangwon 24341, Republic of Korea. e-mail: cjhemd@kangwon.ac.kr or Professor Ji Hyeon Ahn, PhD: Department of Physical Therapy, College of Health Science, Youngsan University, Yangsan, Gyeongnam 50510, Republic of Korea. e-mail: jh-ahn@ysu.ac.kr

www.hh.um.es. DOI: 10.14670/HH-18-840

Introduction

Clinical studies have reported that increased body temperature early after ischemic stroke is significantly related to an increase in infarct volume, which indicates

a higher risk of poor clinical outcomes (de Jonge et al., 2019). In animal studies, changes in body temperature before, during, and after ischemia are critical determinants of the severity of ischemic brain damage (Corbett and Thornhill, 2000). Post-ischemic hypothermia further exerts a neuroprotective effect on the hippocampal CA1 region following *in vivo* transient forebrain ischemia (Minamisawa et al., 1990; Colbourne and Corbett, 1994; Wood et al., 2016), whereas hyperthermia caused by external heat or pyrogens aggravates neuronal damages after *in vivo* transient forebrain ischemia (Dietrich et al., 1990; Minamisawa et al., 1990; Satoh et al., 2011). Mechanisms by which hyperthermia exacerbates ischemic injury include increased oxygen radical production, glutamate release, and metabolic rate (Corbett and Thornhill, 2000).

Brain ischemia and reperfusion (IR) triggers oxygen and glucose deprivation due to the significant decrease or cessation of cerebral blood flow, while the significant production of reactive oxygen species and disruption of redox homeostasis (antioxidative defense capacity) result in brain damage (Chen et al., 2011). During cerebral IR, multiple detrimental processes occur, including oxidant overproduction, detoxification system inactivation, and antioxidant consumption, destroying the antioxidative defense ability of cerebral cells or tissues (Chan, 2001). In laboratory animals with ischemic brain damage, antioxidant proteins, mainly superoxide dismutase (SOD), play a role in oxidative stress (Chen et al., 2011). Numerous studies have shown that SOD enzymes are involved in protecting against brain IR injury (IRI) (Chan, 2001).

Glutamate is an excitatory neurotransmitter involved in neural functions, including learning and memory, in the brain (Myhrer, 2003). Under normal physiological conditions, glutamate is released from presynaptic neurons into the synaptic cleft and is mainly eliminated by cellular uptake, which is necessary to maintain glutamate concentrations below toxic levels (Camacho and Massieu, 2006). It is well known that the regulation of the extracellular glutamate concentration is mediated by glutamate transporters. Among these, glutamate transporter 1 (GLT1), also known as excitatory amino acid transporter 2 (EAAT2), is a main glutamate transporter expressed in neurons and astrocytes (Ketheeswaranathan et al., 2011; Krzyżanowska et al., 2014). In particular, GLT1 in astrocytes is responsible for the extracellular glutamate uptake by astrocytes (Anderson and Swanson, 2000). When glutamate transporters fail to clear excessively increased extracellular glutamate levels after ischemia, neuronal death occurs due to glutamate excitotoxicity (Camacho and Massieu, 2006).

Previous studies have reported that IR under hyperthermic conditions induces excessive damage to neurons and/or astrocytes in gerbil hippocampus (Kim et al., 2015a; Lee et al., 2017; Ohk et al., 2020; Lee et al., 2022). However, the underlying mechanisms exacerbating ischemic neuronal damage under hyperthermia remain unknown. Therefore, in the present study, we aimed to investigate the changes in oxidative stress factors (8OHdG, an oxidative stress nuclear marker; SOD2, an endogenous antioxidant enzyme), an excitotoxic factor (GLT1, a glutamate transporter), and astrogliosis (GFAP, a marker of astrocytes) in the hippocampal CA1 region following IRI (5 min of transient forebrain ischemia) under hyperthermic vs. normothermic conditions to elucidate their roles in the deterioration of hyperthermic ischemia-induced neuronal damage.

Materials and methods

Ethics statement and experimental animals

Adult male gerbils (*Meriones unguiculatus*) weighing 60-70 g (six months old) were obtained from the animal house of the Experimental Animal Center Kangwon National University; Chuncheon, Republic of Korea). Animals were housed under conventional room conditions (temperature, 23±2°C; humidity, 56±5%; light/dark cycle, 12:12) with freely accessible water and food. Animal care was in accordance with the NIH Guide for the Care and Use of Laboratory Animals (National Research Council, 2010). The experimental procedures were approved (approval number, KW-200113-1) by the Institutional Animal Care and Use Committee (IACUC, a committee of Kangwon National University) on January 13, 2020. To minimize animal suffering, the animals were anesthetized before the painful procedure and euthanized before regaining consciousness. In addition, the minimum sample size was determined through power analysis (G*power 3.1) with an effect size of 0.8 and a significance level of 0.05.

Experimental animals (total n=158) were randomly assigned to four groups as follows: normothermia (NT)/sham group, received sham operation under normothermia (n=38); NT/IRI group, received IRI under normothermia (n=41); hyperthermia(HT)/sham group, received sham operation under hyperthermia (n=38); and 4) HT/IRI group, received IRI under hyperthermia (n=41). For immunohistochemistry, five animals per group were sacrificed at designated times (0, 3, 6, 12, 24, 48, and 120h after sham or IRI operation). For western blotting, three animals per group were sacrificed at designated times (0h after sham operation and 24 and 120h after IRI operation) (Fig. 1).

Induction of forebrain IRI and control of body temperature

IRI induction in gerbil forebrains under normothermia or hyperthermia was performed according to previously described methods (Kim et al., 2015a; Lee et al., 2017; Ohk et al., 2020; Lee et al., 2022). The animals were anesthetized with isoflurane (2.5%; Baxtor, Deerfield, IL, USA) using an inhalation anesthesia machine (Harvard Apparatus, Holliston, MA, USA).

Under anesthesia, body temperature was modulated before and during the IRI surgery using heating pads connected to rectal thermistors (homeothermic monitoring system; Harvard Apparatus, Holliston, MA, USA). Body temperature was controlled at 37.0±0.5°C for normothermia and elevated to 39.5±0.2°C for hyperthermia for 30 min before and during the IRI surgery. For IRI induction, the gerbils were in the supine position and the hair on the neck was removed. Bilateral common carotid arteries were isolated from the carotid sheath and ligated using nontraumatic aneurysm clips for 5 min, showing delayed neuronal death in the hippocampal CA1 region with almost no mortality (Kirino and Sano, 1984; Lee et al., 2019). After IRI surgery, the animals were maintained in thermal incubators (temperature, 23±2°C; humidity, 56±5%) to adjust body temperature (normothermic level). Sham animals received the same surgical procedure without the ligation of the arteries.

Preparation of brain sections for histofluorescence and immunohistochemistry

Brain sections containing the hippocampi were prepared as follows. As in previously described methods (Kim et al., 2015a; Lee et al., 2017; Ohk et al., 2020; Lee et al., 2022), the animals were deeply anesthetized with 220 mg/kg sodium pentobarbital at designated times (at 0, 3, 6, 12, 24, 48, and 120h after sham or IRI operation) (Kanda, 2015). The death of animals was confirmed according to vital signs including heartbeat, pupillary response, and respiratory pattern (lack of cardiac activity for 5 min by cardiac palpation, unresponsiveness to light with dilated pupils using light into the eyes of the animal, and lack of spontaneous breathing pattern with shallow and irregular breathing pattern). Under anesthesia, gerbils were transcardially perfused with 4% paraformaldehyde. Immediately, the brains were removed and fixed for 5h. Thereafter, the sections were soaked in 30% sucrose to prevent tissue from freezing. Finally, frontal sections of 30 μm of thickness were made in a cryostat.

Histofluorescence with Fluoro-Jade B (FJB)

FJB histofluorescence (a representative marker of neuronal degeneration or death) staining was conducted to examine IRI-induced neuronal death. As described previously (Kim et al., 2015a; Lee et al., 2017; Schmued and Hopkins, 2000), in brief, tissues were soaked in 0.06% potassium permanganate and reacted with 0.0004% FJB (Histochem, Jefferson, AR, USA) for 50 min at room temperature.

To evaluate FJB-positive neurons, the FJB-stained CA1 region was observed using a Carl Zeiss fluorescence microscope (Göttingen, Germany). Five sections/animal were randomly chosen. Digital images of FJB-positive cells were captured and analyzed using NIH Image J 1.59 software. Cell counting was conducted by averaging the total number of the cells in a 250 μm^2 area at the center of the stratum pyramidale.

Immunohistochemistry

An immunohistochemistry assay was used to examine changes in the expression of neuronal nuclear antigen (NeuN, a marker for neurons), 8-hydroxy-2'-deoxyguanosine (8OHdG, a marker of oxidative DNA damage), superoxide dismutase 2 (SOD2, a marker of endogenous antioxidant enzymes), glutamate transporter 1 (GLT1) for excitotoxicity, and glial fibrillary acidic protein (GFAP) for reactive astrogliosis in gerbil hippocampal CA1 region after IRI. As described previously (Kim et al., 2015a,b; Yang et al., 2019), the sections were blocked with hydrogen peroxide solution and normal goat serum. The sections were then incubated with primary antibodies: mouse anti-NeuN (diluted 1:1100; Chemicon International, Temecula, CA, USA), goat anti-8OHdG (diluted 1:600; Millipore, Billerica, MA, USA), rabbit anti-SOD2 (diluted 1:1000; Abcam, Cambridge, UK), rabbit anti-GLT-1 (diluted 1:1600; Abcam), and mouse anti-GFAP (diluted 1:1100; Chemicon International). This was followed by the secondary antibodies: biotinylated horse anti-mouse IgG, rabbit anti-goat IgG, and goat anti-rabbit IgG (diluted 1:200; Vector, Burlingame, CA, USA) and streptavidin peroxidase complex (diluted 1:250; Vector). Lastly, the sections were visualized with 3,3′-diaminobenzidine tetrahydrochloride to detect the antigen-antibody complex.

Immunoreactive structures or their immunoreactivity were evaluated in five sections at 120 μm intervals/animal. Digital images of NeuN, 8OHdG, SOD2, GLT1, and GFAP immunoreactive structures were taken in

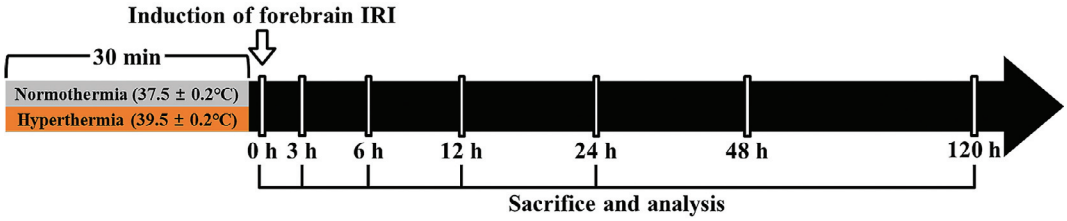

Fig. 1. Experimental design. The body temperature of the gerbils was controlled at normothermic (37.5±0.2°C) or hyperthermic (39.5±0.2°C) conditions for 30 min before and during sham or IRI operation. The gerbils were sacrificed for immunohistochemistry (*n*=5, respectively, 0, 3, 6, 12, 24, 48, and 120h after sham or IRI operation) and western blotting (*n*=3, respectively, 0h after sham operation and 24 and 120h after IRI operation).

regions of interest using an AxioM1 light microscope (Carl Zeiss, Göttingen, Germany). According to published methods (Kim et al., 2015a,b; Yang et al., 2019), the count of NeuN-positive neurons was performed by averaging the total number in 250 μm^2 at the center of the stratum pyramidale of the hippocampal CA1 region, and the relative immuno-reactivity of 8OHdG, SOD2, GLT1 immunoreactive structures in the stratum oriens, pyramidale, and radiatum and GFAP immunoreactive structures in the stratum oriens and radiatum was evaluated as relative optical density (ROD; 100% in sham group) using cellSens Standard software (Olympus) and ImageJ 1.43 software (National Institutes of Health).

Double immunofluorescence

To identify non-pyramidal cells exhibiting SOD2 and GLT1 immunoreactivity, double immuno-fluorescence staining was conducted by a published method (Ohk et al., 2020). Briefly, rabbit anti-SOD2 (diluted 1:500, Abcam) or rabbit anti-GLT1 (diluted 1:1500; Abcam) was used with mouse anti-GFAP (diluted 1:1100; Chemicon International) for astrocytes. The brain sections were reacted with the mixture of the antisera overnight at 4°C, and incubated in the mixture of Alexa Fluor546-conjugated goat anti-rabbit IgG (diluted 1:600; Invitrogen, Carlsbad, CA, USA) and Alexa Fluor488-conjugated goat anti-mouse IgG (diluted 1:600; Invitrogen) for 2 h at room temperature. SOD2 or GLT1/GFAP immunoreactive structures were examined using an LSM-510 META NLO confocal microscope (Carl Zeiss).

Western blotting

To evaluate GLT1 protein levels in the CA1 region, western blotting was conducted by a published method (Ohk et al., 2020). Briefly, three gerbils/group were sacrificed under deep anesthesia by pentobarbital sodium (220 mg/kg, intraperitoneal injection; JW Pharmaceutical Co., Ltd., Seoul, Korea,) at designated times (0h after sham operation and 24 and 120h after IRI) after confirmation of death according to the method described above. The brains of the gerbils were immediately removed and the CA1 tissues were selected to homogenize and ultracentrifuge to collect supernatants. The protein concentration was qualified using the Pierce Bicinchoninic acid (BCA) Protein Assay Kit (Thermos Fisher Scientific Korea Ltd., Seoul, Korea). A 40 μg protein sample was separated by SDS-PAGE and transferred to nitrocellulose membranes obtained from the Pall Corporation (Pittsburgh, PA, USA). Thereafter, the membranes were blocked with 5% bovine serum albumin for 1 hour at room temperature and incubated with primary antibodies; rabbit anti-GLT1 (62 kDa, diluted 1:5000; Abcam) and rabbit anti-β-actin (42 kDa, diluted 1:5,000; Abcam) overnight at 4°C. Finally, the membranes were exposed to peroxidase-conjugated goat anti-rabbit IgG (diluted 1:4,500; Santa Cruz Biotechnology) for 1 hour at room temperature and visualized using enhanced chemiluminescence (ECL) kit (GE Healthcare Life Sciences, Chalfont, UK).

Densitometry analysis was conducted to quantify the bands using ImageJ 1.43 software (National Institutes of Health). The ratio, as the relative density of GLT1 protein was calibrated with the corresponding expression rate of β-actin and normalized to that of the NT/sham group at 0h.

Statistical analysis

The statistical analysis was conducted using SPSS 18.0 (SPSS, Chicago, IL, USA). The significance level was set at p=0.05. Analysis of variance (ANOVA) was selected for differences in means among the groups, and a *post hoc* test (Bonferroni's multiple comparison test) was carried out when statistically significant results were obtained. The values are presented in charts as the mean ± standard deviation.

Results

Effects of hyperthermia on neuronal cell death following IRI

NeuN-immunoreactive neurons

In the NT/sham group, NeuN immunoreactivity in the hippocampal CA1 region was primarily found in the nuclei of pyramidal neurons, known as principal neurons, which constitute the stratum pyramidale (Fig. 2A). In the NT/IRI groups, 48h after IRI, the morphology of NeuN-immunoreactive neurons did not differ from that of the NT/sham group (Fig. 2B,G); however, 120 h after IRI, a few NeuN-immunoreactive neurons were detected in the stratum pyramidale: the number of NeuN-immunoreactive neurons was 18% of that found in the NT/sham group (Fig. 2C,G).

In the CA1 region of the HT/sham group, the number of NeuN-immunoreactive neurons was similar to that in the NT/sham group (Fig. 2D). In the HT/IRI group, 48h after IRI, the number of NeuN immuno-reactive neurons was significantly decreased (45% of the NT/sham group) (Fig. 2E,G), and 120h after IRI, NeuN-immunoreactive neurons in the stratum pyramidale were even more significantly decreased (15% of the NT/sham group) (Fig. 2F,G).

FJB-positive (degenerating) neurons

In the NT/sham group, FJB-positive neurons, which are known as degenerating or dead neurons, were not observed in the CA1 region (Fig. 2a). No FJB-positive neurons were found in the CA1 region in the NT/IRI group 48h after IRI (Fig. 2b); however, 120h after IRI, numerous FJB-positive neurons (mean number, 45.9±1.0/250 μm^2) were identified in the stratum pyramidale, showing FJB histofluorescence in the cell bodies, dendrites, and axons of degenerating neurons

(Fig. 2c,g).

Similar to the NT/sham group, no FJB-positive neurons were observed in the HT/sham group (Fig. 2d). However, in the HT/IRI group, 48h after IRI, many FJB-positive neurons (42.8±1.0/250 μm^2) were identified in the stratum pyramidale (Fig. 2e,g), and, 120h after IRI, a huge number of FJB-positive neurons (46.9±1.0/250 μm^2) were identified in the stratum pyramidale (Fig. 2f,g).

Effects of hyperthermia on oxidative stress following IRI

8OHdG (a marker of oxidative DNA damage)-immunoreactive neurons

In the CA1 region of the NT/sham group, weak 8OHdG immunoreactivity was predominantly detected in the nuclei of pyramidal neurons (CA1 pyramidal neurons) in the stratum pyramidale (Fig. 3A). In the NT/IRI group, 8OHdG immunoreactivity in the CA1 pyramidal neurons was significantly increased compared with the NT/sham group, with a maximum increase of 332.4% relative to the NT/sham group 48h after IRI (Fig. 3B-F,O); conversely, 120h after IRI, very low 8OHdG immunoreactivity (30.8% of the NT/sham group) was shown in the CA1 pyramidal neurons, due to the loss of CA1 pyramidal cells (Fig. 3G,O).

In CA1 pyramidal neurons of the HT/sham group, strong 8OHdG immunoreactivity was identified compared with the NT/sham group (166.6% of the NT/sham group) (Fig. 3H,O). In the HT/IRI group, 8OHdG immunoreactivity in the pyramidal neurons was significantly increased (350.9% of the NT/sham group) from 3h, peaking (486.1% of the NT/sham group) 24h after IRI (Fig. 3I-L,O). Thereafter, 48 and 120h after IRI, 8OHdG immunoreactivity in pyramidal neurons

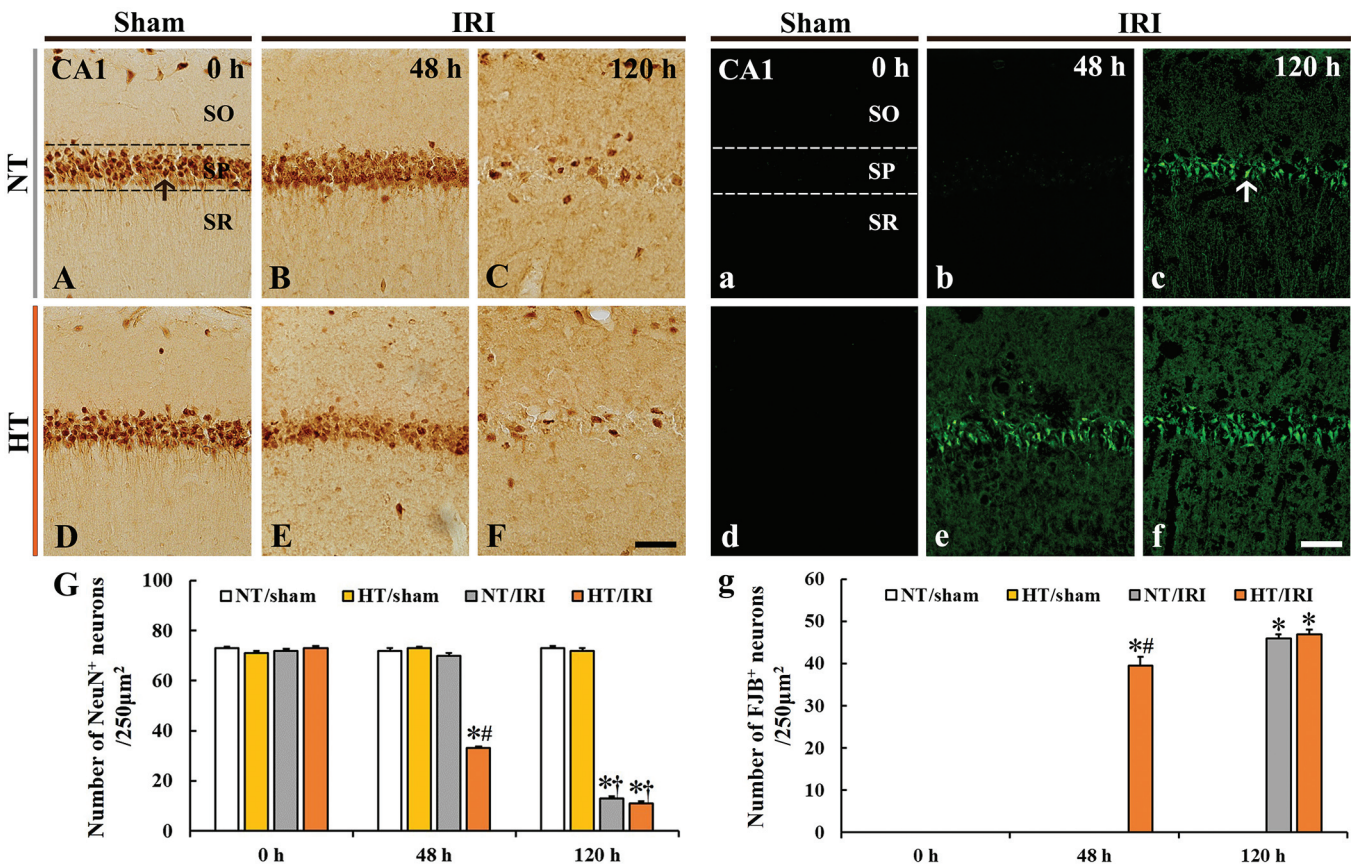

Fig. 2. A-F and a-f. NeuN immunohistochemistry and FJB histofluorescence staining in the CA1 region of the NT/sham **(A, a)**, NT/IRI **(B, C, b, c)**, HT/sham **(D, d)**, and HT/IRI **(E, F, e, f)** groups 0h after sham operation and 48 and 120h after IRI. In the NT/sham group, numerous NeuN-immunoreactive neurons (arrow in **A**) are observed, however, in the NT/IRI group, a significant loss of NeuN-immunoreactive neurons (in **C**) isobserved in the stratum pyramidale 120h after IRI. In the HT/IRI group, NeuN immunoreactivity is reduced (in **E**) 48 h after IRI, and a few NeuN-immunoreactive neurons are detected (in **F**) 120h after IRI. Many FJB-positive pyramidal neurons are detected (arrow in **c**) 120h after IRI. In the HT/IRI group, many FJB-positive pyramidal neurons are observed (in **e** and **f**) 48 and 120 h after IRI. SO, stratum oriens; SP, stratum pyramidale; SR, stratum radiatum. Scale bar: 50 μm. **G, g.** Numbers of NeuN-immunoreactive **(G)** and FJB-positive **(g)** neurons in the CA1 region. *p<0.05 vs. NT/sham group at 0h; $^{\dagger}p$<0.05 vs. group at pre-time point; $^{\#}p$<0.05 vs. corresponding NT/IRI group. The bars indicate means ± SEM (n=5/group at each point in time).

was significantly reduced (187.2% and 33.3% of the NT/sham group, respectively) due to damage/death of the CA1 pyramidal neurons (Fig. 3M-3O).

Compared with the NT/IRI group, 8OHdG immunoreactivity in the HT/IRI group was significantly higher from 6h to 24h after IRI but significantly lower 48 h after IRI (Fig. 3O).

SOD2 (a marker of endogenous antioxidant enzymes) immunoreactivity

SOD2 immunoreactivity in the CA1 region of the NT/sham group was primarily detected in the cytoplasm and dendrites of pyramidal neurons in the stratum pyramidale (Fig. 4A). In the NT/IRI group, SOD2 immunoreactivity in the CA1 pyramidal neurons was significantly decreased 3 and 6h after IRI (37.5% and 32.2% of the NT/sham group, respectively) (Fig. 4B,C,P), increased 12h after IRI (141.2% of the NT/sham group), and again decreased 24, 48, and 120 h after IRI (43.9%, 66.7%, and 393.7% of the NT/sham group, respectively) (Fig. 4D-G,P). In particular, SOD2 immunoreactivity 120h after IRI was observed in non-pyramidal cells located in the stratum oriens and radiatum (Fig. 4G).

In the HT/sham group, significantly increased SOD2 immunoreactivity (272.9% of the NT/sham group) was identified in CA1 pyramidal neurons (Fig. 4H,P). In the HT/IRI group, the increased SOD2 immunoreactivity in CA1 pyramidal neurons gradually reduced (236.8%, 166.3%, 121.1%, and 38.1% of the NT/sham group 3, 6, 12, and 24h after IRI, respectively) until 24h after IRI (Fig. 4I-L,P). At 48h after IRI, SOD2 immunoreactivity increased again (113.1% of the NT/sham group) (Fig. 4M,P). In particular, 120h after IRI, SOD2 immunoreactivity was significantly increased in non-pyramidal cells (434.5% of the NT/sham group) (Fig. 4N,P).

Compared with the NT/IRI group, SOD2 immunoreactivity in the HT/IRI group was significantly higher 3, 6, and 48h after IRI (Fig. 4P).

In this study, SOD2 immunoreactivity was detected in non-pyramidal cells located in the stratum oriens and radiatum of the sham groups and IRI groups 6 h after IRI under normothermic and hyperthermic conditions. To identify the cell type, double immunofluorescence staining for GFAP (an astrocyte maker)/SOD2 revealed that SOD2-immunoreactive non-pyramidal cells were merged with GFAP-immunoreactive astrocytes in the NT/sham, HT/sham, NT/IRI, and HT/IRI groups (Fig. 4O).

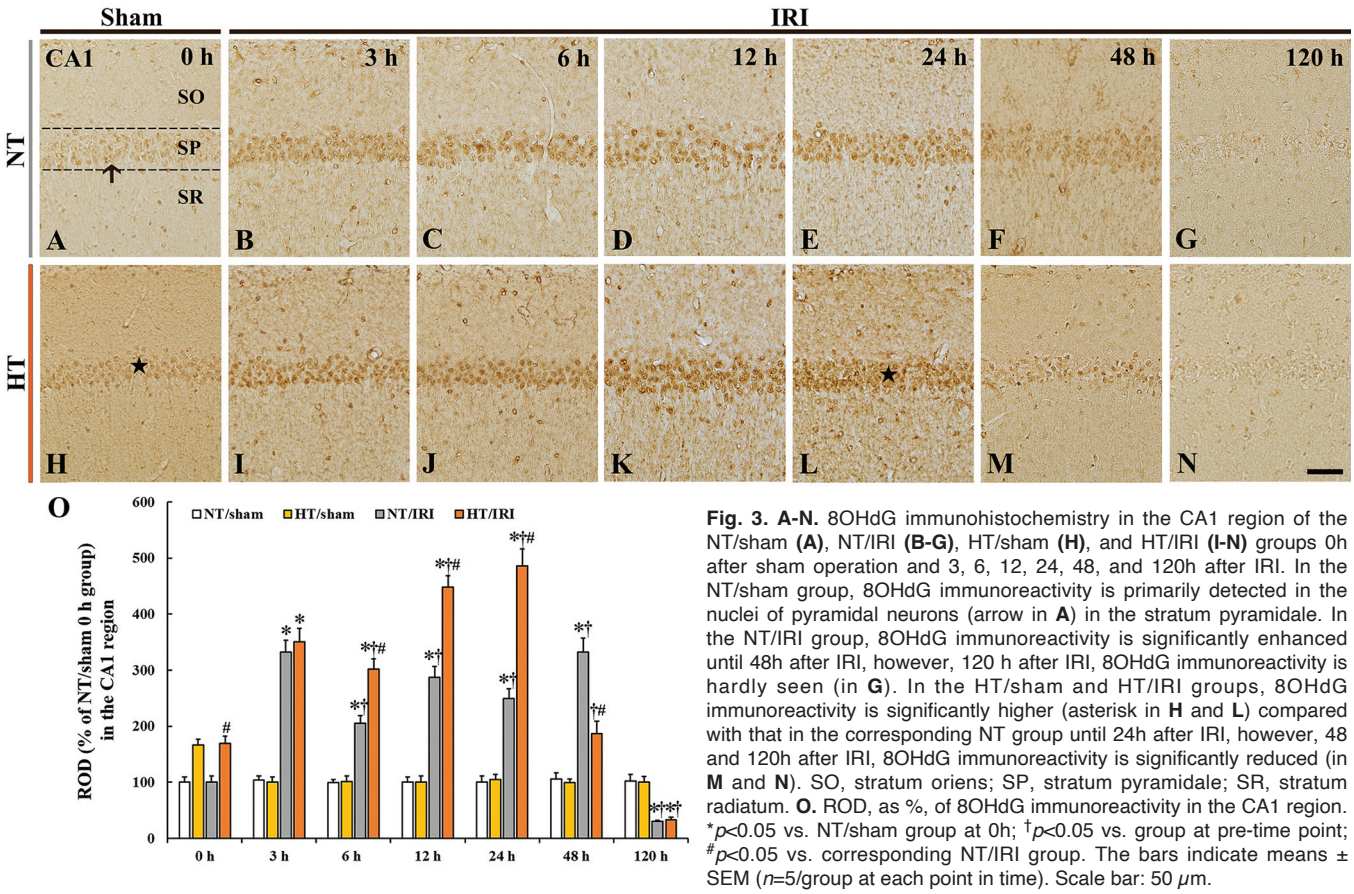

Fig. 3. A-N. 8OHdG immunohistochemistry in the CA1 region of the NT/sham **(A)**, NT/IRI **(B-G)**, HT/sham **(H)**, and HT/IRI **(I-N)** groups 0h after sham operation and 3, 6, 12, 24, 48, and 120h after IRI. In the NT/sham group, 8OHdG immunoreactivity is primarily detected in the nuclei of pyramidal neurons (arrow in **A**) in the stratum pyramidale. In the NT/IRI group, 8OHdG immunoreactivity is significantly enhanced until 48h after IRI, however, 120 h after IRI, 8OHdG immunoreactivity is hardly seen (in **G**). In the HT/sham and HT/IRI groups, 8OHdG immunoreactivity is significantly higher (asterisk in **H** and **L**) compared with that in the corresponding NT group until 24h after IRI, however, 48 and 120h after IRI, 8OHdG immunoreactivity is significantly reduced (in **M** and **N**). SO, stratum oriens; SP, stratum pyramidale; SR, stratum radiatum. **O.** ROD, as %, of 8OHdG immunoreactivity in the CA1 region. *p<0.05 vs. NT/sham group at 0h; †p<0.05 vs. group at pre-time point; #p<0.05 vs. corresponding NT/IRI group. The bars indicate means ± SEM (n=5/group at each point in time). Scale bar: 50 μm.

Effects of hyperthermia on excitotoxicity following IRI

GLT1 immunoreactivity

In the CA1 region of the NT/sham group, GLT1 immunoreactivity was observed in the stratum pyramidale containing pyramidal neuron bodies, as well as in the stratum radiatum containing the dendrites of pyramidal neurons (Fig. 5A). In the NT/IRI group, GLT1 immunoreactivity in the CA1 region was significantly decreased 3 and 6h after IRI (52.7% and 46.3% of the NT/sham group, respectively) (Fig. 5B,C,P), while at 12, 24, and 48h after IRI, GLT1 immunoreactivity was increased (94.8%, 84.1%, and 67.5% of the NT/sham group, respectively) (Fig. 5D-F,P). At 120h after IRI, GLT1 immunoreactivity was dramatically reduced (9.1% of the NT/sham group) (Fig. 5G,P); nevertheless, weak GLT1 immunoreactivity was observed in non-pyramidal cells (Fig. 5G).

In the HT/sham group, the distribution pattern of GLT1 immunoreactivity in the CA1 region did not differ from that of the NT/sham group, however, GLT1

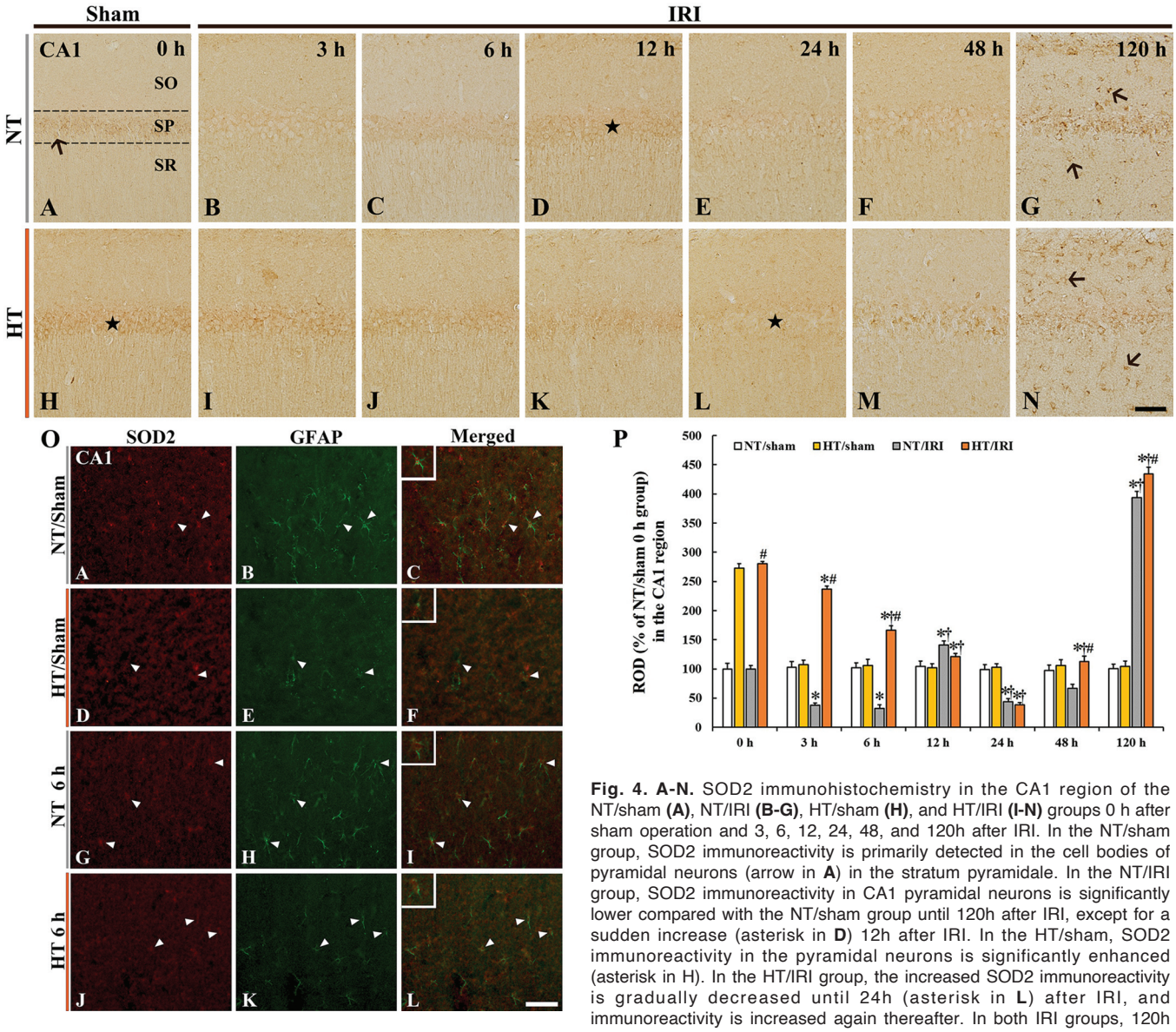

Fig. 4. A-N. SOD2 immunohistochemistry in the CA1 region of the NT/sham **(A)**, NT/IRI **(B-G)**, HT/sham **(H)**, and HT/IRI **(I-N)** groups 0 h after sham operation and 3, 6, 12, 24, 48, and 120h after IRI. In the NT/sham group, SOD2 immunoreactivity is primarily detected in the cell bodies of pyramidal neurons (arrow in **A**) in the stratum pyramidale. In the NT/IRI group, SOD2 immunoreactivity in CA1 pyramidal neurons is significantly lower compared with the NT/sham group until 120h after IRI, except for a sudden increase (asterisk in **D**) 12h after IRI. In the HT/sham, SOD2 immunoreactivity in the pyramidal neurons is significantly enhanced (asterisk in H). In the HT/IRI group, the increased SOD2 immunoreactivity is gradually decreased until 24h (asterisk in **L**) after IRI, and immunoreactivity is increased again thereafter. In both IRI groups, 120h after IRI, strong SOD2 immunoreactivity is observed in non-pyramidal cells (arrows in **G** and **N**). SO, stratum oriens; SP, stratum pyramidale; SR, stratum radiatum. **O.** Double immunofluorescence staining for SOD2 (red), GFAP (green), and merged images at 0 h after sham operation and 6 h after IRI in the NT/IRI and HT/IRI groups. SOD2 immunoreactivity is merged with GFAP-immunoreactive astrocytes (arrowheads). **P.** ROD, as %, of SOD2 immunoreactivity in the CA1 region. *p<0.05 vs. NT/sham group at 0h; †p<0.05 vs. group at pre-time point; #p<0.05 vs. corresponding NT/IRI group. The bars indicate means ± SEM (n=5/group at each point in time). Scale bar: 50 μm.

immunoreactivity was significantly lower (71.3% of the NT/sham group) (Fig. 5H,P). In the HT/IRI group, the change in the pattern of GLT1 immunoreactivity was similar to that in the NT/IRI group, however, GLT1 immunoreactivity was decreased 3, 6, 12, 24, 48, and 120h after IRI (50.1%, 38.8%, 52.1%, 32.8%, 57.1%, and 45.2% of the NT/sham group, respectively) until 120h after IRI (Fig. 5I-N,P).

Compared with the NT/IRI group, GLT1 immunoreactivity in the HT/IRI group was significantly lower 12 and 24h after IRI but markedly higher 120h after IRI (Fig. 5P).

In this study, GLT1 immunoreactivity was detected in non-pyramidal cells located in the stratum oriens and radiatum of the sham and IRI groups 6h after IRI under normothermic and hyperthermic conditions. The GLT1-immunoreactive non-pyramidal cells were identified as GFAP-immunoreactive astrocytes in the NT/sham, HT/sham, NT/IRI, and HT/IRI groups (Fig. 5O).

GLT1 protein level

Changes in the protein level of GLT1 in the CA1 region were similar to those observed in the ROD investigating GLT1 immunoreactivity (Fig. 6). In the NT/IRI group, GLT1 protein levels were significantly

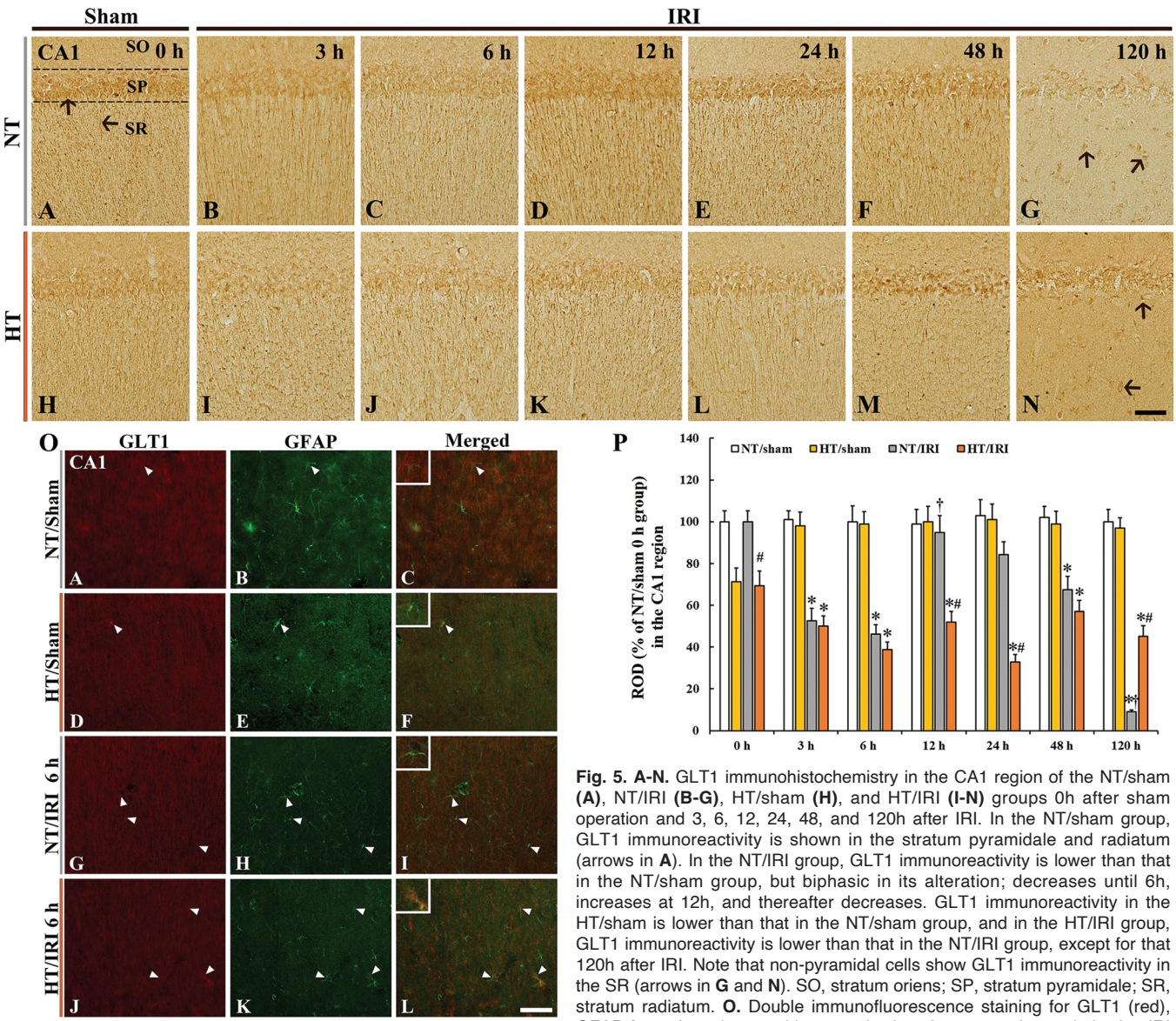

Fig. 5. A-N. GLT1 immunohistochemistry in the CA1 region of the NT/sham **(A)**, NT/IRI **(B-G)**, HT/sham **(H)**, and HT/IRI **(I-N)** groups 0h after sham operation and 3, 6, 12, 24, 48, and 120h after IRI. In the NT/sham group, GLT1 immunoreactivity is shown in the stratum pyramidale and radiatum (arrows in **A**). In the NT/IRI group, GLT1 immunoreactivity is lower than that in the NT/sham group, but biphasic in its alteration; decreases until 6h, increases at 12h, and thereafter decreases. GLT1 immunoreactivity in the HT/sham is lower than that in the NT/sham group, and in the HT/IRI group, GLT1 immunoreactivity is lower than that in the NT/IRI group, except for that 120h after IRI. Note that non-pyramidal cells show GLT1 immunoreactivity in the SR (arrows in **G** and **N**). SO, stratum oriens; SP, stratum pyramidale; SR, stratum radiatum. **O.** Double immunofluorescence staining for GLT1 (red), GFAP (green), and merged images 0h after sham operation and 6h after IRI in the NT/IRI and HT/IRI groups. GLT1 immunoreactivity is localized to GFAP-immunoreactive astrocytes (arrowheads). **P.** ROD, as %, of GLT1 immunoreactivity in the CA1 region. *p<0.05 vs. NT/sham group at 0h; †p<0.05 vs. group at pre-time point; #p<0.05 vs. corresponding NT/IRI group. The bars indicate means ± SEM (n=5/group at each point in time). Scale bar: 50 μm.

decreased 24h and 120h after IRI (76.0% and 19.9% of the NT/sham group, respectively) (Fig. 6).

In the HT/sham group, GLT1 protein levels were significantly decreased (76.5 % of the NT/sham group) (Fig. 6). In the HT/IRI group, 24h after IRI, the protein level of GLT1 was significantly lower (23.1% of the NT/sham group) (Fig. 6). At 120h after IRI, the decrease in GLT1 protein levels was maintained (34.6% of the NT/sham group) in the HT/IRI group (Fig. 6).

Compared with the NT/IRI group, the GLT1 protein level in the HT/IRI group was significantly lower 24h after IRI but there was no significant difference 120h after IRI (Fig. 6).

Effects of hyperthermia on reactive astrogliosis following IRI

GFAP immunoreactivity

In the NT/sham group, GFAP-immunoreactive astrocytes, typically characterized by small cell bodies and thin processes, were distributed throughout the hippocampal CA1 region (Fig. 7A). In the NT/IRI group, GFAP-immunoreactive astrocytes, as reactive astroglia, displayed enlarged cell bodies and elongated processes until 12h after IRI, indicating a significant increase in GFAP immunoreactivity 3, 6, and 12h after IRI (176.9%, 300.1%, and 286.2% of the NT/sham group, respectively) (Fig. 7B-D,O). At 24h after IRI, GFAP immunoreactivity was decreased (158.8% of the NT/sham group) (Fig. 7E,O), after which GFAP immunoreactivity was significantly and gradually increased 48 and 120h after IRI (268.1% and 822.2% of the NT/sham group, respectively) (Fig. 7F,G,O). At these time points, many GFAP-immunoreactive astrocytes had enlarged cytoplasm as well as thickened and shortened processes (Fig. 7E-G).

GFAP-immunoreactive astrocytes in the HT/sham group did not differ from those in the NT/sham group (Fig. 7H). In the HT/IRI group, 3h after IRI, GFAP-immunoreactive astrocytes presented larger cytoplasmic regions and thicker processes, and a significant increase (240.4% of the NT/sham group) in GFAP immunoreactivity was observed (Fig. 7I,O). Conversely, GFAP immunoreactivity was decreased 6 and 12h after IRI (200.3% and 168.2% of the NT/sham group, respectively) (Fig. 7J,K,O). GFAP immunoreactivity was significantly and gradually increased 24, 48, and 120h after IRI (251.9%, 515.2%, and 1144.6% of the NT/sham group, respectively) (Fig. 7L-O). In particular, 48 and 120h after IRI, the cytoplasm was hypertrophied, and the processes were short, thick, and blunt (Fig. 7M,N).

Compared with the NT/IRI group, GFAP immunoreactivity in the HT/IRI group was significantly higher 3, 24, 48, and 120h after IRI but lower 12h after IRI (Fig. 7O).

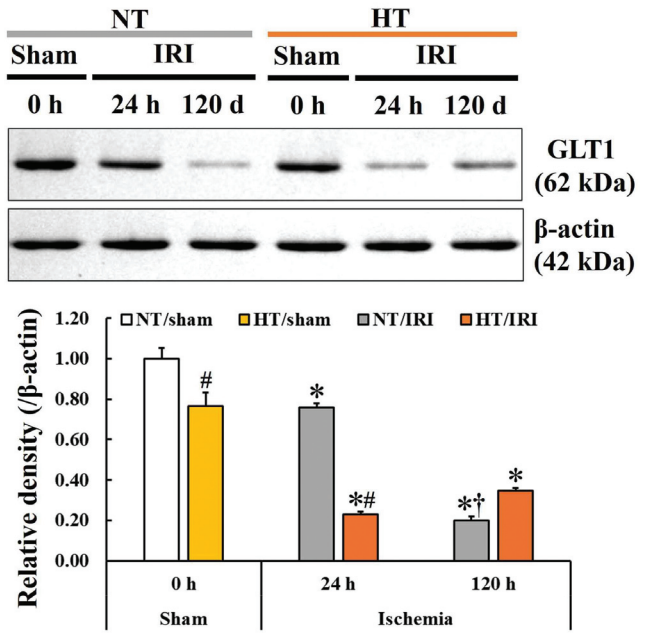

Fig. 6. Western blot analysis of GLT1 in the CA1 region of the NT/sham, NT/IRI, HT/sham, and HT/IRI groups 0h after sham operation and 24 and 120h after IRI. The relative density of representative western blot bands is represented. The protein level of GLT1 is normalized to β-actin. The error bars indicate means ± SEM (n=3/group; *p<0.05 vs. corresponding NT/sham group at 0h; †p<0.05 vs. group at pre-time point; #p<0.05 vs. corresponding NT/IRI).

Discussion

This study investigated the mechanisms underlying the acceleration of neuronal damage in the gerbil hippocampal CA1 region following transient forebrain ischemia for 5 min, indicating the presence of IR in the forebrain, under hyperthermic conditions. These mechanisms include changes in 8OHdG and SOD2 for oxidative stress, GLT1 for excitotoxicity, and GFAP for reactive astrocytes.

It is well known that 5-min transient forebrain ischemia in gerbils induces the death of CA1 pyramidal cells (principal neurons) 96 to 120h after IR, resulting in a loss of this population (Kirino, 1982; Yu et al., 2012). In this study, we observed the same findings in the CA1 region of the NT/IRI group using NeuN immunohistochemistry and FJB histofluorescence; our analysis showed that the HT/IRI group had a more rapid induction of neuronal cell death (48h after IRI) than the NT/IRI group (120h after IRI). These results are consistent with previous findings (Kim et al., 2015a; Lee et al., 2017, 2022), and similar to those of previous studies showing that intra-ischemic hyperthermia markedly accelerates and exacerbates IR-induced neuronal damage/loss in the rodent hippocampal CA1 region (Dietrich et al., 1990; Minamisawa et al., 1990; Satoh et al., 2011). These findings suggest that the timing and extent of neuronal death in the hippocampal

CA1 region after 5-min transient forebrain ischemia may be significantly affected by hyperthermia.

In the present study, 8OHdG immunoreactivity, the most representative product of DNA oxidation among all indicators of oxygen radical-mediated damage, dramatically changed over time after IRI under normothermic or hyperthermic conditions. IR in the gerbil forebrain further resulted in the accumulation of DNA oxidation in CA1 pyramidal neurons until the loss of neurons after IRI in both the NT/IRI and HT/IRI groups, showing that hyperthermia significantly increased 8OHdG immunoreactivity in CA1 pyramidal neurons compared with the NT/IRI group. Our findings in the NT/IRI group are consistent with previous studies showing that oxidation markers, including 8OHdG, were significantly increased in the gerbil hippocampus following global ischemia (Park et al., 2000; Miyamoto et al., 2003), and that the levels of 8OHdG and advanced oxidation protein products (AOPP) were increased in human plasma following exposure to hypoxia (Pialoux et al., 2009). This finding is supported by previous studies reporting that hyperthermia during transient global ischemia further increased the accumulation of hydroxyl radicals (OH•), and malondialdehyde (MDA, a lipid peroxidation marker) in the brain parenchyma during ischemia and recirculation (reperfusion) in rats (Globus et al., 1995; Kil et al., 1996; Zhang et al., 2014). Taken together, our results indicate that oxidative DNA damage is significantly increased following IRI, and that hyperthermia can further increase DNA oxidation, thereby exacerbating the death of CA1 pyramidal neurons after 5 min of transient forebrain ischemia (IR in the forebrain).

IRI is a serious clinical event. In both clinical practice and experimental studies, ischemia itself does not cause significant harm to cells/tissues/organs; instead, excess reactive oxygen species (ROS) damage or destroy cells as blood circulation is restored, the shock of which directly triggers further tissue and organ damage (Wu et al., 2018). It has also been reported that oxidative DNA damage can be generated by superoxide anions ($\bullet O_2^-$) that subsequently promote the formation of hydroxyl radicals (OH•) by transferring electrons to hydrogen peroxide (H_2O_2) (Keyer et al., 1995; Keyer and Imlay, 1996). Furthermore, in mouse brains with IRI, SOD2 mRNA and protein levels are reduced, which occurs concomitantly with the overproduction $\bullet O_2^-$, and plays an important role in ischemic neuronal death after IR (Jung et al., 2009). Mammals express abundant endogenous antioxidant enzymes, including SODs,

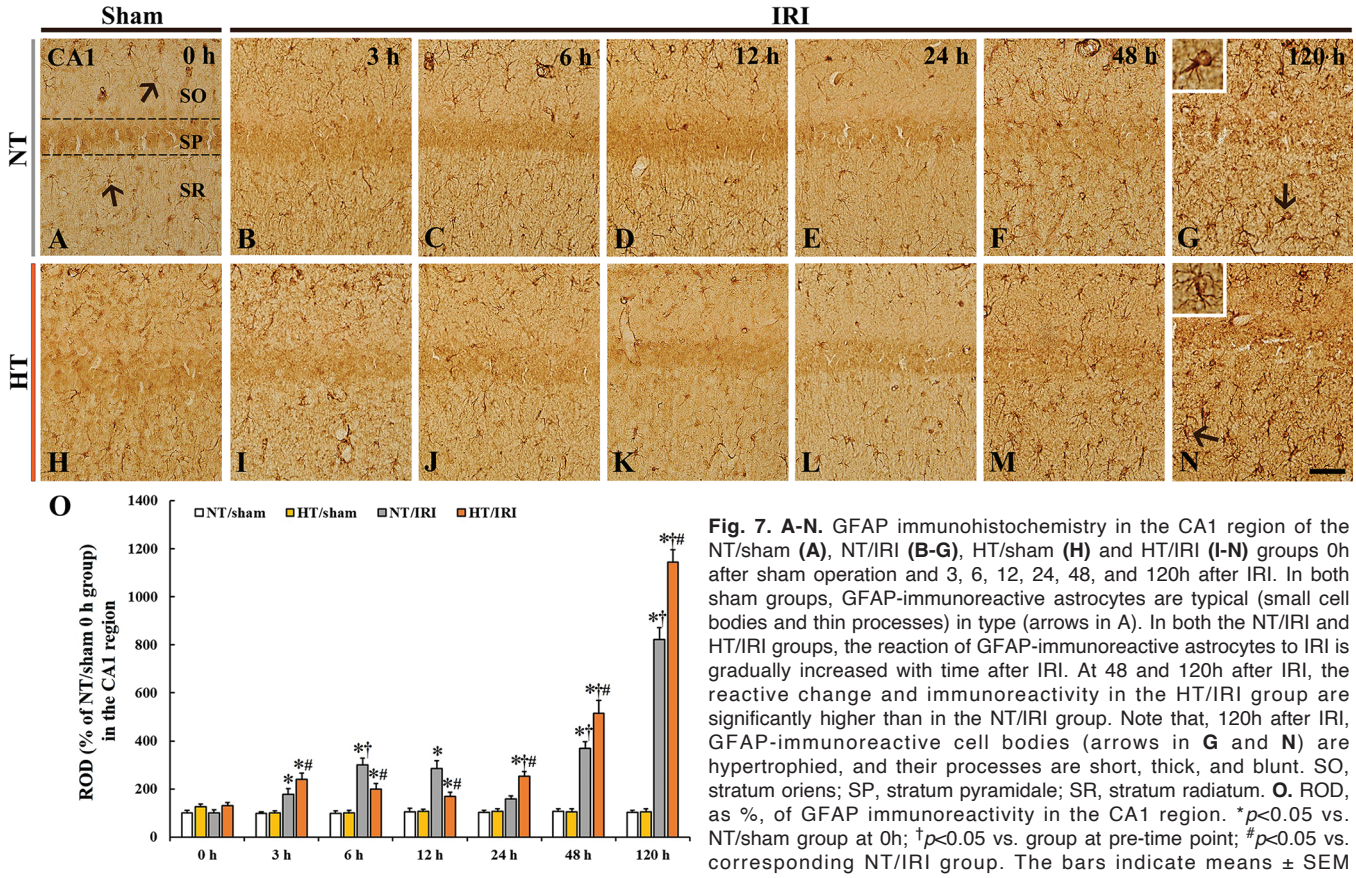

Fig. 7. A-N. GFAP immunohistochemistry in the CA1 region of the NT/sham **(A)**, NT/IRI **(B-G)**, HT/sham **(H)** and HT/IRI **(I-N)** groups 0h after sham operation and 3, 6, 12, 24, 48, and 120h after IRI. In both sham groups, GFAP-immunoreactive astrocytes are typical (small cell bodies and thin processes) in type (arrows in A). In both the NT/IRI and HT/IRI groups, the reaction of GFAP-immunoreactive astrocytes to IRI is gradually increased with time after IRI. At 48 and 120h after IRI, the reactive change and immunoreactivity in the HT/IRI group are significantly higher than in the NT/IRI group. Note that, 120h after IRI, GFAP-immunoreactive cell bodies (arrows in **G** and **N**) are hypertrophied, and their processes are short, thick, and blunt. SO, stratum oriens; SP, stratum pyramidale; SR, stratum radiatum. **O.** ROD, as %, of GFAP immunoreactivity in the CA1 region. *p<0.05 vs. NT/sham group at 0h; †p<0.05 vs. group at pre-time point; #p<0.05 vs. corresponding NT/IRI group. The bars indicate means ± SEM (n=5/group at each point in time). Scale bar: 50 μm.

glutathione peroxidase, and catalase, to alleviate oxidative damage following IRI (McMichael and Moore, 2004; Chen et al., 2011). Therefore, in the present study, we investigated changes in the immunoreactivity of SOD2, which is crucial in ischemic cells (Asimakis et al., 2002), in the CA1 region of NT/IRI and HT/IRI gerbils.

In our analysis, we found that SOD2 immunoreactivity in CA1 pyramidal neurons of the NT/IRI group was significantly reduced in the early phase after IR, whereas the immunoreactivity of the HT/sham group was more than 2.5 times that in the NT/IRI group. Additionally, in the HT/IRI group, SOD2 immunoreactivity in the early phase after IR was significantly higher than that of the NT/IRI group, although the immunoreactivity gradually decreased with time after IR. Interestingly, 24h after IRI, the lowest SOD2 immunoreactivity and the highest 8OHdG immunoreactivity were observed in the HT/IRI group, which may be related to earlier CA1 pyramidal neuron death after IRI under hyperthermic conditions (Kim et al., 2015a; Lee et al., 2017; Ohk et al., 2020). Our findings are related to a report showing that higher total antioxidant capacity (TAC) and lipid peroxidation levels were identified in the serum of non-survivors compared to survivors of ischemic stroke (Lorente et al., 2016), with one paper reporting further hyperthermia-induced rapid elevations in the mRNA and protein levels of antioxidants in ischemic rat brains as a defense mechanism against heat shock stress (Ewing et al., 1992). Taken together, these results suggest that SOD2 immunoreactivity is further increased in brain cells following IR under exacerbated conditions, such as hyperthermia, to compensate for the high oxidative DNA stress induced by cerebral IR.

It is well known that astrocytes and/or neurons have to remove excessive glutamate from the extracellular space to protect neurons from glutamate excitotoxicity (Verma et al., 2010). In the case of ischemic insults, failure to eliminate increased extracellular glutamate following cerebral ischemia can lead to neuronal death by glutamate excitotoxicity (Camacho and Massieu, 2006; Krzyżanowska et al., 2014). Astrocytic glutamate transporters play a crucial role in the removal of extracellular glutamate (Rothstein et al., 1996; Rose et al., 2018). Mitani and Tanaka (2003) reported that, in GLT1-mutant mice, the increase in glutamate levels in the hippocampus during 5-min ischemia was higher than that in wild-type mice, while the glutamate level remained high in the early phase after reperfusion, leading to pyramidal cell death in the CA1 region 24h after IRI (Mitani and Tanaka, 2003). One possible mechanism underlying this glutamate transport dysfunction is that increased free radical production after IRI leads to the oxidation of glutamate transporters, which are susceptible to oxidation due to their thiol/disulfide-based redox regulatory regions, thereby resulting in reduced glutamate uptake (Trotti et al., 1998; McBean, 2017). In the present study, GLT1 immunoreactivity in CA1 pyramidal neurons was biphasically decreased in the NT/IRI group; however, GLT1 immunoreactivity in the HT/IRI group was continuously and significantly lower than that in the NT/IRI group. In addition, the western blot results for GLT1 protein levels were similar to those of GLT1 immunohistochemistry. In a mouse model of focal ischemic stroke induced by middle cerebral artery occlusion, GLT-1 mRNA expression was found to be significantly decreased in the cerebral cortex compared with sham-operated brains (Ketheeswaranathan et al., 2011). In addition, GLT1 protein expression in the gerbil hippocampus following 10-min transient forebrain ischemia was decreased by 36% in the early phase after ischemia (Yu et al., 2012), while GLT1 protein expression in rat hippocampus following 20-min transient global cerebral ischemia was decreased by 20% 6h after ischemia (Kirino, 1982). In previous studies, decreased GLT1 expression was observed before extensive neuronal death induced by IRI; this finding is similar to our present results. Taken together, these results suggest that reduced GLT1 expression as a consequence of oxidative damage to the glutamate transporter after IRI is responsible for the loss of CA1 pyramidal neurons, and that hyperthermia induces the acceleration of CA1 pyramidal neuronal death by greater GLT1 reduction after IRI.

Astrocytes undergo adaptive changes in morphology, molecular expression, proliferation, and scar formation after ischemic stroke in a progressive process referred to as reactive astrogliosis (Panickar and Norenberg, 2005; He et al., 2022). In a gerbil model of transient forebrain ischemia, immunohistochemical staining for GFAP, a major intermediate filament and astrocyte marker (Tanigami et al., 2005), found that reactive astrocytes have an enlarged cytoplasm, thickened processes, and damaged end-feet in the ischemic CA1 region (Park et al., 2018; Kim et al., 2019; Shin et al., 2022). In the present study, GFAP immunoreactivity in the CA1 region was gradually increased, peaking 120h post-IRI in both the NT/IRI and HT/IRI groups, indicating that the reaction (astrogliosis) was significantly higher in the HT/IRI group than in the NT/IRI group. Consistent with our findings, a previous study reported that GFAP immunoreactivity and mRNA levels in the mouse hippocampal CA1 region were significantly increased, peaking 96h after IR (Ketheeswaranathan et al., 2011). In addition, in a previous study, we and our colleagues reported that in gerbils, more severe reactive astrogliosis (higher GFAP immunoreactivity and an increased number of astrocytes) could be observed after severe ischemic conditions, including hyperthermia (Kim et al., 2015a), increased ischemic duration (Yan et al., 2014a; Lee et al., 2019), or a high-fat diet (Yan et al., 2014b). Reactive astrocytes interact with neurons and are deeply involved in either neuronal protective (including antioxidant and anti-excitatory defenses and metabolic support) or damage (brain edema and neuroinflammation) responses, depending on the post-ischemic context and phase (He et al., 2022). In terms of

molecular expression in ischemic astrocytes, in the present study, SOD2 and GLT1 were expressed in non-pyramidal cells in the NT/sham, HT/sham, NT/IRI, and HT/IRI groups. Double immunofluorescence staining to identify the cell type revealed that GFAP-positive astrocytes were merged with SOD2- and/or GLT1-immunoreactive cells, indicating that astrocytes are involved in the regulation of antioxidant enzymes and glutamate transporters following IRI. Taken together, these results suggest that astrocytes exhibit changes in morphology and GFAP expression such as reactive astrogliosis, after IRI, and that IR under hyperthermic conditions results in more severe astrogliosis.

In summary, our results showed earlier neuronal damage, higher 8OHdG and SOD2 immunoreactivity, lower GLT1 immunoreactivity and protein levels, and stronger GFAP immunoreactivity in the CA1 region of the hippocampus in the HT/IRI group compared with the NT/IRI group. In addition, not only pyramidal neurons but also astrocytes expressed SOD2 and GLT1, indicating that activated astrocytes after IRI are also involved in the regulation of oxidative stress and excitotoxicity in the hippocampal CA1 region following IRI under hyperthermic conditions.

Conclusion

Taken together, the results of this study suggest that hippocampal CA1 neurons undergo more severe or accelerated neuronal damage following IRI under hyperthermic conditions when compared with normothermic conditions, which is closely associated with excessive DNA oxidation, despite a significant increase in SOD2 expression (indication of oxidative stress), a significant reduction in GLT1 expression (indication of excitotoxicity), and a significant increase in GFAP expression (indication of astrogliosis) in hippocampal CA1 neurons and/or astrocytes in the early phase after IRI.

Acknowledgements. The authors would like to thank Mr. Seung Uk Lee and Ms. Hyun Sook Kim for their technical help in this work.

Funding. This research was supported by the Basic Science Research Program through the National Research Foundation of Korea (NRF) funded by the Ministry of Education (NRF-2021R1A2C1094224, NRF-2022R1F1A1065996, and RS-2023-00245858).

Compliance with Ethics Approval. The experimental procedures were approved (Approval number, KW-200113-1) by the Institutional Animal Care and Use Committee (IACUC, a committee of Kangwon National University) on January 13, 2020. Every effort was made to minimize animal suffering and the numbers of animals were minimized.

Availability of data and materials. All data generated or analyzed during this study are included in this published article.

Competing Interest. All authors declare no competing interest.

References

Anderson C.M. and Swanson R.A. (2000). Astrocyte glutamate transport: Review of properties, regulation, and physiological functions. Glia 32, 1-14.

Asimakis G.K., Lick S. and Patterson C. (2002). Postischemic recovery of contractile function is impaired in SOD2$^{+/-}$ but not SOD1$^{+/-}$ mouse hearts. Circulation 105, 981-986.

Camacho A. and Massieu L. (2006). Role of glutamate transporters in the clearance and release of glutamate during ischemia and its relation to neuronal death. Arc. Med. Res. 37, 11-18.

Chan P.H. (2001). Reactive oxygen radicals in signaling and damage in the ischemic brain. J. Cereb. Blood Flow Metab. 21, 2-14.

Chen H., Yoshioka H., Kim G.S., Jung J.E., Okami N., Sakata H., Maier C.M., Narasimhan P., Goeders C.E. and Chan P.H. (2011). Oxidative stress in ischemic brain damage: Mechanisms of cell death and potential molecular targets for neuroprotection. Antioxid. Redox Signal. 14, 1505-1517.

Colbourne F. and Corbett D. (1994). Delayed and prolonged post-ischemic hypothermia is neuroprotective in the gerbil. Brain Res. 654, 265-272.

Corbett D. and Thornhill J. (2000). Temperature modulation (hypothermic and hyperthermic conditions) and its influence on histological and behavioral outcomes following cerebral ischemia. Brain Pathol. 10, 145-152.

National Research Council. (2010). Guide for the care and use of laboratory animals. 8th ed. Nat. Acad. Press.

de Jonge J.C., Wallet J. and van der Worp H.B. (2019). Fever worsens outcomes in animal models of ischaemic stroke: A systematic review and meta-analysis. Eur. Stroke J. 4, 29-38.

Dietrich W.D., Busto R., Valdes I. and Loor Y. (1990). Effects of normothermic versus mild hyperthermic forebrain ischemia in rats. Stroke 21, 1318-1325.

Ewing J., Haber S. and Maines M. (1992). Normal and heat-induced patterns of expression of heme oxygenase-1 (HSP32) in rat brain: Hyperthermia causes rapid induction of mRNA and protein. J. Neurochem. 58, 1140-1149.

Globus M.Y.T., Busto R., Lin B., Schnippering H. and Ginsberg M.D. (1995). Detection of free radical activity during transient global ischemia and recirculation: Effects of intraischemic brain temperature modulation. J. Neurochem. 65, 1250-1256.

He T., Yang G.-Y. and Zhang Z. (2022). Crosstalk of astrocytes and other cells during ischemic stroke. Life 12, 910.

Jung J.E., Kim G.S., Narasimhan P., Song Y.S. and Chan P.H. (2009). Regulation of Mn-superoxide dismutase activity and neuroprotection by stat3 in mice after cerebral ischemia. J. Neurosci. 29, 7003-7014.

Kanda I. (2015). Exotic animal formulary. Can. Vet. J. 56, 736.

Ketheeswaranathan P., Turner N.A., Spary E.J., Batten T.F., McColl B.W. and Saha S. (2011). Changes in glutamate transporter expression in mouse forebrain areas following focal ischemia. Brain Res. 1418, 93-103.

Keyer K. and Imlay J.A. (1996). Superoxide accelerates DNA damage by elevating free-iron levels. Proc. Natl. Acad. Sci. USA 93, 13635-13640.

Keyer K., Gort A.S. and Imlay J.A. (1995). Superoxide and the production of oxidative DNA damage. J. Bacteriol. 177, 6782-6790.

Kil H.Y., Zhang J. and Piantadosi C.A. (1996). Brain temperature alters hydroxyl radical production during cerebral ischemia/reperfusion in rats. J. Cereb. Blood Flow Metab. 16, 100-106.

Kim M.J., Cho J.H., Park J.H., Ahn J.H., Tae H.J., Cho G.S., Yan B.C., Hwang I.K., Lee C.H., Bae E.J., Won M.H. and Lee J.C. (2015a). Impact of hyperthermia before and during ischemia-reperfusion on

neuronal damage and gliosis in the gerbil hippocampus induced by transient cerebral ischemia. J. Neurol. Sci. 348, 101-110.

Kim D.W., Cho J.-H., Cho G.-S., Kim I.H., Park J.H., Ahn J.H., Chen B.H., Shin B.-N., Tae H.-J. and Hong S. (2015b). Hyperthermic preconditioning severely accelerates neuronal damage in the gerbil ischemic hippocampal dentate gyrus via decreasing SODs expressions. J. Neurol. Sci. 358, 266-275.

Kim H., Park J.H., Shin M.C., Cho J.H., Lee T.-K., Kim H., Song M., Park C.W., Park Y.E. and Lee J.-C. (2019). Fate of astrocytes in the gerbil hippocampus after transient global cerebral ischemia. Int. J. Mol. Sci. 20, 845.

Kirino T. (1982). Delayed neuronal death in the gerbil hippocampus following ischemia. Brain Res. 239, 57-69.

Kirino T. and Sano K. (1984). Selective vulnerability in the gerbil hippocampus following transient ischemia. Acta. Neuropathol. 62, 201-208.

Krzyżanowska W., Pomierny B., Filip M. and Pera J. (2014). Glutamate transporters in brain ischemia: To modulate or not? Acta. Pharmacol. Sin. 35, 444-462.

Lee J.-C., Cho J.-H., Lee T.-K., Kim I.H., Won M.-H., Cho G.-S., Shin B.-N., Hwang I.K., Park J.H. and Ahn J.H. (2017). Effect of hyperthermia on calbindin-d 28k immunoreactivity in the hippocampal formation following transient global cerebral ischemia in gerbils. Neural Regen. Res. 12, 1458.

Lee T.-K., Kim H., Song M., Lee J.-C., Park J.H., Ahn J.H., Yang G.E., Kim H., Ohk T.G. and Shin M.C. (2019). Time-course pattern of neuronal loss and gliosis in gerbil hippocampi following mild, severe, or lethal transient global cerebral ischemia. Neural Regen. Res. 14, 1394.

Lee T.-K., Kim D.W., Sim H., Lee J.-C., Kim H.I., Shin M.C., Cho J.H., Park J.H., Lee C.-H. and Won M.-H. (2022). Hyperthermia accelerates neuronal loss differently between the hippocampal CA1 and CA2/3 through different hif-1α expression after transient ischemia in gerbils. Int. J. Mol. Med. 49, 1-10.

Lorente L., Martín M.M., Pérez-Cejas A., Abreu-González P., Ramos L., Argueso M., Cáceres J.J., Solé-Violán J. and Jiménez A. (2016). Association between total antioxidant capacity and mortality in ischemic stroke patients. Ann. Intensive Care 6, 1-6.

McBean G.J. (2017). Cysteine, glutathione, and thiol redox balance in astrocytes. Antioxidants 6, 62.

McMichael M. and Moore R.M. (2004). Ischemia–reperfusion injury pathophysiology, part I. J. Vet. Emerg. Crit. Care 14, 231-241.

Minamisawa H., Smith M.L. and Siesjo B.K. (1990). The effect of mild hyperthermia and hypothermia on brain damage following 5, 10, and 15 minutes of forebrain ischemia. Ann. Neurol. 28, 26-33.

Mitani A. and Tanaka K. (2003). Functional changes of glial glutamate transporter GLT-1 during ischemia: An in vivo study in the hippocampal ca1 of normal mice and mutant mice lacking GLT-1. J. Neurosci. 23, 7176-7182.

Miyamoto O., Tamae K., Kasai H., Hirakawa H., Hayashida Y., Konishi R. and Itano T. (2003). Suppression of hyperemia and DNA oxidation by indomethacin in cerebral ischemia. Eur. J. Pharmacol. 459, 179-186.

Myhrer T. (2003). Neurotransmitter systems involved in learning and memory in the rat: A meta-analysis based on studies of four behavioral tasks. Brain Res. Rev. 41, 268-287.

Ohk T.G., Ahn J.H., Park Y.E., Lee T.K., Kim B., Lee J.C., Cho J.H., Park J.H., Won M.H. and Lee C.H. (2020). Comparison of neuronal death and expression of TNF-α and MCT4 in the gerbil hippocampal CA1 region induced by ischemia/reperfusion under hyperthermia to those under normothermia. Mol. Med. Rep. 22, 1044-1052.

Panickar K.S. and Norenberg M.D. (2005). Astrocytes in cerebral ischemic injury: Morphological and general considerations. Glia 50, 287-298.

Park J.H., Noh Y., Kim S.-S., Ahn J.H., Ohk T.G., Cho J.H., Lee T.-K., Kim H., Song M. and Lee J.-C. (2018). Time-course changes and new expressions of MIP-3α and its receptor, CCR6, in the gerbil hippocampal CA1 area following transient global cerebral ischemia. Neurochem. Res. 43, 2102-2110.

Park E.-M., Choi J.-H., Park J.-S., Han M.-Y. and Park Y.-M. (2000). Measurement of glutathione oxidation and 8-hydroxy-2′-deoxyguanosine accumulation in the gerbil hippocampus following global ischemia. Brain Res. Protoc. 6, 25-32.

Pialoux V., Mounier R., Brown A.D., Steinback C.D., Rawling J.M. and Poulin M.J. (2009). Relationship between oxidative stress and HIF-1α mrna during sustained hypoxia in humans. Free Radic. Biol. Med. 46, 321-326.

Rose C.R., Felix L., Zeug A., Dietrich D., Reiner A. and Henneberger C. (2018). Astroglial glutamate signaling and uptake in the hippocampus. Front. Mol. Neurosci. 10, 451.

Rothstein J.D., Dykes-Hoberg M., Pardo C.A., Bristol L.A., Jin L., Kuncl R.W., Kanai Y., Hediger M.A., Wang Y. and Schielke J.P. (1996). Knockout of glutamate transporters reveals a major role for astroglial transport in excitotoxicity and clearance of glutamate. Neuron 16, 675-686.

Satoh K., Niwa M., Binh N.H., Nakashima M., Kobayashi K., Takamatsu M. and Hara A. (2011). Increase of galectin-3 expression in microglia by hyperthermia in delayed neuronal death of hippocampal CA1 following transient forebrain ischemia. Neurosci. Lett. 504, 199-203.

Schmued L.C. and Hopkins K.J. (2000). Fluoro-jade B: A high affinity fluorescent marker for the localization of neuronal degeneration. Brain Res. 874, 123-130.

Shin M.C., Lee T.-K., Lee J.-C., Kim H.I., Park C.W., Cho J.H., Kim D.W., Ahn J.H., Won M.-H. and Lee C.-H. (2022). Therapeutic effects of stiripentol against ischemia-reperfusion injury in gerbils focusing on cognitive deficit, neuronal death, astrocyte damage and blood brain barrier leakage in the hippocampus. Korean J. Physiol. Pharmacol. 26, 47-57.

Tanigami H., Rebel A., Martin L., Chen T.-Y., Brusilow S., Traystman R. and Koehler R. (2005). Effect of glutamine synthetase inhibition on astrocyte swelling and altered astroglial protein expression during hyperammonemia in rats. Neuroscience 131, 437-449.

Trotti D., Danbolt N.C. and Volterra A. (1998). Glutamate transporters are oxidant-vulnerable: A molecular link between oxidative and excitotoxic neurodegeneration? Trends. Pharmacol. Sci. 19, 328-334.

Verma R., Mishra V., Sasmal D. and Raghubir R. (2010). Pharmacological evaluation of glutamate transporter 1 (GLT-1) mediated neuroprotection following cerebral ischemia/reperfusion injury. Eur. J. Pharmacol. 638, 65-71.

Wood T., Osredkar D., Puchades M., Maes E., Falck M., Flatebø T., Walløe L., Sabir H. and Thoresen M. (2016). Treatment temperature and insult severity influence the neuroprotective effects of therapeutic hypothermia. Sci. Rep. 6, 23430.

Wu M.-Y., Yiang G.-T., Liao W.-T., Tsai A.P.-Y., Cheng Y.-L., Cheng P.-W., Li C.-Y. and Li C.-J. (2018). Current mechanistic concepts in ischemia and reperfusion injury. Cell Physiol. Biochem. 46, 1650-

1667.

Yan B.C., Ohk T.G., Ahn J.H., Park J.H., Chen B.H., Lee J.-C., Lee C.H., Shin M.C., Hwang I.K. and Moon S.M. (2014a). Differences in neuronal damage and gliosis in the hippocampus between young and adult gerbils induced by long duration of transient cerebral ischemia. J. Neurol. Sci. 337, 129-136.

Yan B.C., Park J.H., Ahn J.H., Kim I.H., Lee J.-C., Yoo K.-Y., Choi J.H., Hwang I.K., Cho J.H. and Kwon Y.-G. (2014b). Effects of high-fat diet on neuronal damage, gliosis, inflammatory process and oxidative stress in the hippocampus induced by transient cerebral ischemia. Neurochem. Res. 39, 2465-2478.

Yang G.E., Tae H.-J., Lee T.-K., Park Y.E., Cho J.H., Kim D.W., Park J.H., Ahn J.H., Ryoo S. and Kim Y.-M. (2019). Risperidone treatment after transient ischemia induces hypothermia and provides neuroprotection in the gerbil hippocampus by decreasing oxidative stress. Int. J. Mol. Sci. 20, 4621.

Yu D.-K., Yoo K.-Y., Shin B.N., Kim I.H., Park J.H., Lee C.H., Choi J.H., Cho Y.-J., Kang I.-J. and Kim Y.-M. (2012). Neuronal damage in hippocampal subregions induced by various durations of transient cerebral ischemia in gerbils using fluoro-jade B histofluorescence. Brain Res. 1437, 50-57.

Zhang H., Li L., Xu G.-y., Mei Y.-w., Zhang J.-j., Murong S.-x., Sun S.-g. and Tong E.-t. (2014). Changes of c-fos, malondialdehyde and lactate in brain tissue after global cerebral ischemia under different brain temperatures. J. Huazhong Univ. Sci. Technolog. Med. Sci. 34, 354-358.

Accepted October 29, 2024